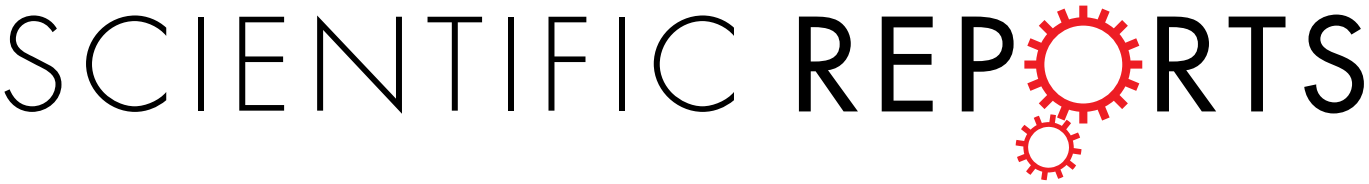

OPEN

Atomistic switch of giant magnetoresistance and spin thermopower in graphene-like nanoribbons

Received: 22 July 2016
Accepted: 20 October 2016
Published: 18 November 2016

Ming-Xing Zhai[1,2] & Xue-Feng Wang[1,3]

We demonstrate that the giant magnetoresistance can be switched off (on) in even- (odd-) width zigzag graphene-like nanoribbons by an atomistic gate potential or edge disorder inside the domain wall in the antiparallel (*ap*) magnetic configuration. A strong magneto-thermopower effect is also predicted that the spin thermopower can be greatly enhanced in the ap configuration while the charge thermopower remains low. The results extracted from the tight-binding model agree well with those obtained by first-principles simulations for edge doped graphene nanoribbons. Analytical expressions in the simplest case are obtained to facilitate qualitative analyses in general contexts.

The giant magnetoresistance (GMR) effect, which is discovered in sandwiched structures of magnetic and nonmagnetic materials in 1988[1,2], means that a large conductance difference turns up when the relative spin orientation in adjacent magnetic materials change from parallel (*p*) to antiparallel (*ap*). GMR is essential in some spintronic devices that manipulate electron spin rather than charge[3] and has led to the explosive enlargement of storage capability on hard disk in the last decades, reflecting its important value in commercial applications.

Charge and spin thermopower of a material describes the ability to produce charge and spin current, respectively, from a temperature gradient rather than a voltage one. Charge thermopower devices such as thermocouple have been widely used in our daily life. Spin thermopower has been observed in magnetic[4] and nonmagnetic[5] materials and should have application potential in spintronics. Similar to the GMR effect, the thermopower in magnetic junctions can change when the magnetic configuration changes from *p* to *ap* and lead to the magneto-thermopower phenomena[6]. The GMR and thermopower effects are both intrinsically relevant to the transmission spectrum in tunneling junctions. Recently, magnetoresistance[7–13] and spin thermopower[13–16] in graphene-like nanoribbons have become one of the focuses.

The discovery of graphene and its many outstanding properties[17] has inspired enormous attentionon graphene-like two-dimensional (2D) materials. The long spin relaxation time and length in graphene indicates it a prospective material for spintronics[18]. Specially, experimental observations have confirmed the existence of magnetism on zigzag edges of graphene[19,20]. Both theoretical models[20–22] and computational simulations based on *ab initio* density functional theory[23,24] have shown that the magnetism origins from the spin polarized edge atoms. Zigzag graphene nanoribbons (ZGNRs) have two zigzag edges and can be in ferromagnetic (FM) or antiferromagnetic (AFM) state classified by the relative spin orientations on the two edges[20,24]. External magnetic field can convert a ZGNR from its ground insulator AFM state to its metallic FM state. The consequent large colossal magnetoresistance was observed persistent up to room temperature[7]. In addition, GMR in FM ZGNRs of even width has been predicted very high[10] as well as the colossal magnetoresistance[8]. ZGNR based GMR devices are believed very useful based on the fact that ZGNRs can be synthesized and relevant devices fabricated in atomic precision with the state-of-the-art technology[19,20]. Traditional chemical and physical edge functionalizations in atomistic scale such as atom adsorption, doping, vacancy and local lattice distortion have been proposed to manipulate further the properties and design diversified devices[25,26]. Specifically, the edge disorders or defects can break geometry symmetry of ZGNRs and enhance the spin thermopower effect. In addition, scanning tunneling microscopy

[1]Jiangsu Key Laboratory of Thin Films, College of Physics, Optoelectronics and Energy, Soochow University, 1 Shizi Street, Suzhou 215006, China. [2]Hongzhiwei Technology Co. Ltd., 1888 Xinjinqiao Road, Pudong, Shanghai 201206, China. [3]Key Laboratory of Terahertz Solid-State Technology, Shanghai Institute of Microsystem and Information Technology, Chinese Academy of Sciences, 865 Changning Road, Shanghai 200050, China. Correspondence and requests for materials should be addressed to X.-F.W. (email: wxf@suda.edu.cn)

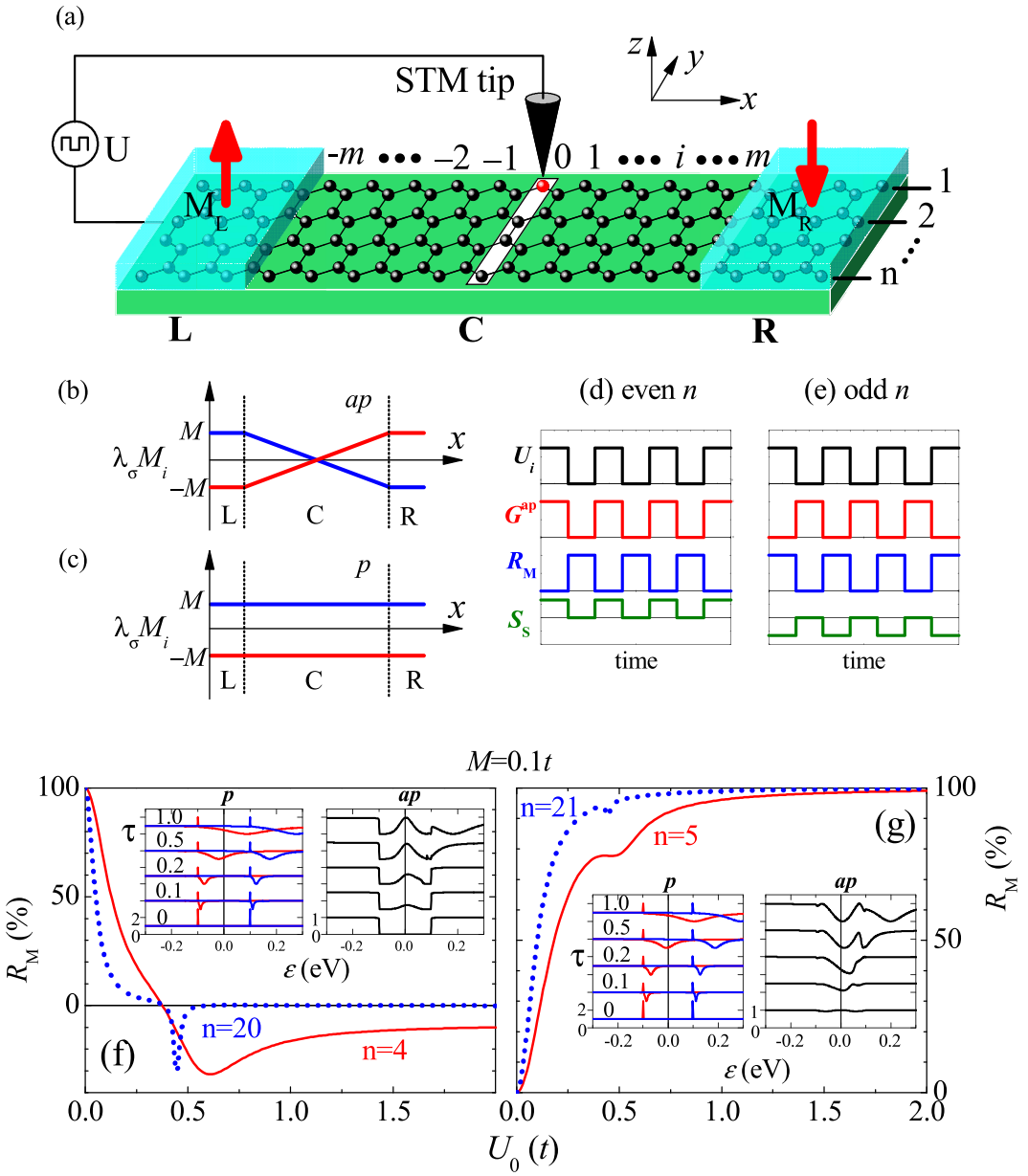

Figure 1. (**a**) Schematic structure of a FM *n*-ZNR two-probe junction with a central region of length 2 *m*. A third probe, the STM tip, can apply a local potential U_i at an edge site $i \in [-m, m]$ to manipulate the magnetoresistance R_M and spin Seebeck coefficient S_S. Edge site 0 (in red) has the minimal magnetization in the *ap* configuration. The colored arrow indicates the spin orientation of the electrodes. (**b,c**) Edge magnetization profile along the *x* direction in the *ap* and *p* configurations, respectively, for up (red) and down (blue) spins. (**d,e**) A possible variation set of G^{ap}, R_M, and S_S with a square-wave signal U_i applied by the STM tip for even and odd *n*, respectively. (**f**) Zero temperature R_M versus U_0 in a 4-ZNR (red) and a 20-ZNR (blue) with $m = 5$ and $M = 0.1\,t$. The left inset shows the transmission spectra $\tau_{\uparrow}^{p}(\varepsilon)$ (red) and $\tau_{\downarrow}^{p}(\varepsilon)$ (blue) under $U_0 = 0$, 0.1, 0.2, 0.5, 1.0 *t* (upward) in a 4-ZNR and the right shows $\tau_{\sigma}^{ap}(\varepsilon)$. (**g**) Same as (f) for odd $n = 5$ (red) and 21 (blue) and the insets for $n = 5$. Note that the spectra for $U_0 \neq 0$ in the insets of (**f,g**) have been shifted upward for clearness and the vertical value of their fact parts is equal to 1.

(STM) tip and atomic force microscopic techniques can be used as atomistic gate to apply local electrostatic potential for graphene transistors and manually introduce and control the disorders[27,28]. In this work, based on the tight-binding model and the first-principles simulations, we propose a mechanism to switch on and off GMR and spin thermopower by applying an atomistic extrinsic potential on edge of FM zigzag nanoribbons (ZNRs) of two-dimensional (2D) graphene-like honeycomb lattice. Our prediction may be confirmed via an experimental setup schemed in Fig. 1 by combining the techniques for measuring the current-voltage curve of narrow nanoribbons[7,29,30] with the STM techniques for controlling the potential in atomistic scale[27,28]. In addition, the effects discussed in the following for single local potential or impurity might be enhanced in disordered systems[31].

Models and Methods

As schemed in Fig. 1(a), we partition a FM ZNR into two-probe devices with left (L) and right (R) electrodes and a central (C) device region (domain wall in the *ap* configuration). A simplified tight-binding Hamiltonian can be used to describe the system[9]

$$H = \sum_{i,\sigma}(U_i + \lambda_\sigma M_i)c^\dagger_{i,\sigma}c_{i,\sigma} - \sum_{i,j,\sigma} t(c^\dagger_{i,\sigma}c_{j,\sigma} + h.c.) \quad (1)$$

here $c^\dagger_{i,\sigma}$ ($c_{i,\sigma}$) is the creation (annihilation) operator of spin σ ($\uparrow$ or $\downarrow$) on site i. t is the nearest-neighbor hopping integral and is chosen as the unit of energy throughout the paper. The uniform on-site energy of the corresponding pristine 2D materials gives the Dirac point energy and is set to zero. U_i and $\lambda_\sigma M_i$ ($\lambda_\uparrow = -1$ and $\lambda_\downarrow = +1$) are the on-site extrinsic potential energy from gate or disorder and the local magnetization, respectively. The magnetizations on the two edges are in parallel and linearly decay to zero from the edges to the center along the y direction. Along the x direction, $\lambda_\sigma M_i$ is constant $\lambda_\sigma M$ (full magnetization) in the electrodes and varies linearly in region C as depicted in Fig. 1(b,c) for the *ap* and *p* magnetic configurations of electrodes, respectively.

In the Landauer-Buttiker formalism with non-coherent effects neglected, the current of spin σ read $I_\sigma = \frac{e}{h}\int d\varepsilon (f^{\mathrm{L}}_\sigma - f^{\mathrm{R}}_\sigma)\tau_\sigma(\varepsilon)$ where $f^{\mathrm{L(R)}}_\sigma$ is the Fermi-Dirac distribution function $f_\sigma = [1 + e^{(\varepsilon-\mu_\sigma)/k_BT}]^{-1}$ in electrode L (R). T and μ_σ are the electron temperature and the Fermi energy. $\tau_\sigma(\varepsilon) = Tr[\Gamma_{\mathrm{L}}(\varepsilon)G^r(\varepsilon)\Gamma_{\mathrm{R}}(\varepsilon)G^a(\varepsilon)]_\sigma$ is the electron transmission calculated by nonequilibrium Green's function (NEGF) method[32]. Here $G^r(\varepsilon) = [G^a(\varepsilon)]^+ = [\varepsilon - h_{\mathrm{C}} - \sum_{\mathrm{L}} - \sum_{\mathrm{R}}]^{-1}$ is the retarded Green's function corresponding to the Hamiltonian h_C in region C and $\Gamma_{\mathrm{L(R)}}(\varepsilon) = i[\sum_{\mathrm{L(R)}} - \sum^+_{\mathrm{L(R)}}]$ is the broadening function. The self-energy function $\sum_{\mathrm{L(R)}}$ due to the coupling between the device and electrode L (R) is obtained via the iterative procedure.

In the linear response regime of small voltage bias ΔV_σ and temperature difference ΔT between the electrodes, we express $\Delta f_\sigma = f^{\mathrm{L}}_\sigma - f^{\mathrm{R}}_\sigma$ in Taylor expansion[33] and have $I_\sigma = G_0K_{0\sigma}(\mu_\sigma, T)\Delta V_\sigma + G_0K_{1\sigma}(\mu_\sigma, T)\Delta T/(eT)$ with $K_{\nu\sigma} = \int d\varepsilon(\varepsilon - \mu_\sigma)^\nu\tau_\sigma(\varepsilon)(\partial f_\sigma/\partial\varepsilon)$ for $\nu = 0$, 1 and the conductance quantum $G_0 = e^2/h$. The tunneling magnetoresistance $R_{\mathrm{M}} = (G^p_t - G^{ap}_t)/(G^p_t + G^{ap}_t)$ of the device is then evaluated[34] from the total linear conductance $G^{p\,(ap)}_t = G_0\sum_\sigma K^{p(ap)}_{0\sigma}$ in the p (ap) configuration. The charge and spin Seebeck coefficients are defined by $S_{\mathrm{C(S)}} = (S_\uparrow \pm S_\downarrow)/2$ with $S_\sigma = -\lim_{\Delta T\to 0}(\Delta V_\sigma/\Delta T) = -K_{1\sigma}(\mu_\sigma, T)K^{-1}_{0\sigma}(\mu_\sigma, T)/(eT)$ when $I_\sigma = 0$[35–38]. At low temperature the Mott formula[35,36] $S_\sigma \overset{\Delta T\to 0}{\approx} -(\pi^2k^2_BT/3e)\tau'_\sigma(\mu_\sigma)/\tau_\sigma(\mu_\sigma)$ applies and analytical results can be obtained in simple cases.

More realistic Hamiltonians for ZNRs of specific materials can be obtained from the density functional theory (DFT) based on first-principles. As an example, we have carried out simulations on magnetoresistance and thermopower for doped n-ZGNRs with width n employing the Atomistic Toolkits (ATK) package[39,40]. The double-ζ plus polarization (DZP) basis set and an energy cutoff of 150 Ry within the local spin density approximation (LSDA) are used in the DFT simulation and a force tolerance of 0.03 eV/Å is set on each atom during the geometry relaxation. We find good agreement between results from the tight-binding model and from the first-principles simulations.

Results and Discussion

We consider ZNR systems of $m = 5$ in the linear response regime with the Fermi energy at the neutral point, i.e. $\mu_\sigma = 0$ throughout the manuscript. The effect of one single impurity on the Fermi energy is assumed negligible. For systems with Fermi energy away from the neutral point, the conductance of the system can be estimated from the energy dependence of transmission. In the p configuration, perfect ZNRs are uniformly magnetized and translationally symmetric along the x direction. The extended edge states have flat bands at the full magnetization energy $\lambda_\sigma M$ near the boundary of the first Brillouin zone. There is one transport channel for each spin σ at $\varepsilon = 0$[9] so $G^p_\sigma = G_0$ for both even and odd n at zero temperature. In the presence of a local extrinsic potential U_{i} at any edge site i, a bound state of energy ε^B_σ appears around the site with $(\varepsilon^B_\sigma - \lambda_\sigma M) \propto U_{\mathrm{i}}$. The bound state can slightly reduce G^p_σ if ε^B_σ is close to zero[41] as illustrated by the transmission spectra τ^p_σ in the left insets of Fig. 1(f,g) where $U_{\mathrm{i}} > 0$. The charge and spin thermopower are both very limited according to the Mott formula.

In the *ap* configuration the conductance becomes much more sensitive to U_{i} and n. We define the site $i = 0$ as the edge site where the magnetization reverses direction in the domain wall. For a geometrically left-right symmetric junction as schemed in Fig. 1(a), the residual magnetization vanishes at site 0, i.e. $M_0 = 0$. In the absence of extrinsic potential U_{i}, we have $G^{ap}_\sigma = 0$ for even n and $G^{ap}_\sigma \approx G_0$ for odd n at zero temperature due to geometry symmetry as indicated in the right insets of Fig. 1(f,g). The corresponding magnetoresistance R_M is about 100% for even n and very small for odd n[10–13,17]. In the presence of U_{i}, we will present the results for $U_{\mathrm{i}} > 0$ in two typical cases, $i = 0$ and $i > 0$ in the following since those for $U_{\mathrm{i}} < 0$ or $i < 0$ can be then deduced based on the symmetry of the systems.

At first we apply a local potential U_0 only at edge site 0 of an n-ZNR. For even n, as shown in the right inset of Fig. 1(f), a transmission peak emerges at $\varepsilon = 0$ with $\tau^{ap}_\sigma(0)$ approaching to unit as U_0 increases. The corresponding R_M, as plotted in Fig. 1(f), then decreases from 100% to near zero and can become negative if G^p_{t} is reduced to $G^p_{\mathrm{t}} < G^{ap}_{\mathrm{t}}$ by the bound state. In contrast, for odd n as illustrated in Fig. 1(g), $\tau^{ap}_\sigma(0)$ decreases inversely with U_0 from unit and approaches to zero, which leads to a jump of R_M from zero to near 100%. When the dip bottom of G^p_{t} due to the bound state passes through the Fermi energy near $U_0 = 0.5\,t$, a R_M minimum appears for both even and odd n.

The conductance and magnetoresistance are also relevant to the full magnetization M which can vary for different materials and/or substrates. In Fig. 2(a,b), we plot G^{ap}_t versus M under $U_0 = t$ for various even and odd n, respectively. In nonmagnetic ZNRs ($M = 0$), $G^{ap}_t \equiv G^p_t \approx 2G_0$ or $R_M = 0$. As M increases, G^{ap}_t decreases gradually

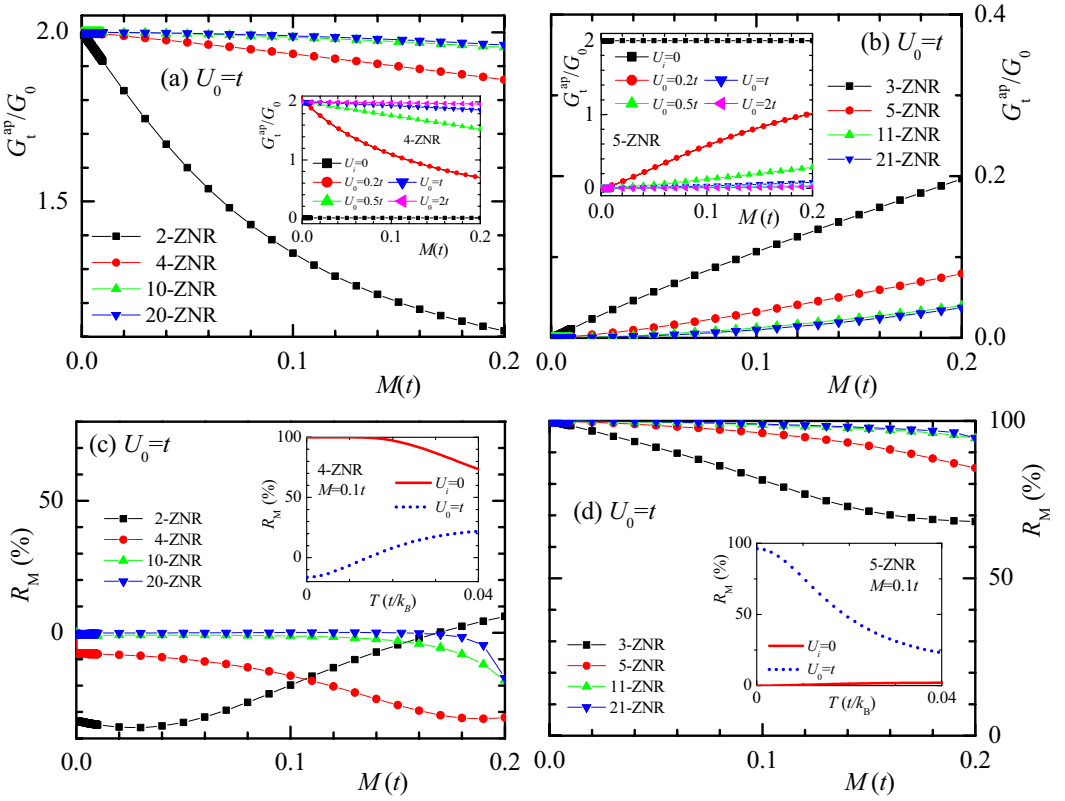

Figure 2. (**a**,**b**) Show the total zero-temperature conductance G_t^{ap} versus the edge magnetization M in the presence of potential $U_0 = t$ at edge site 0 of n-ZNRs for even n (2, 4, 10, 20) and odd n (3, 5, 11, 21), respectively. The corresponding magnetoresistance R_M is illustrated in (**c**,**d**). G_t^{ap} versus M and R_M versus T at $M = 0.1\,t$ are plotted in the insets of the upper and lower panels, respectively, for 4-ZNRs and 5-ZNRs under different U_0. Note that results of $M = 0$ are not shown.

from $2G_0$ but remains high for even n. In contrast, for odd n, G_t^{ap} is very sensitive to M and jumps down to zero once M becomes finite, similar to the behavior of perfect even-width ZNRs[10] as shown in the inset of Fig. 2(a). It then increases monotonically with M but remains in low values. In the range of $M \in [0, 0.2]t$, $G_t^{ap} > G_0$ in 2-ZNRs while $G_t^{ap} < 0.2G_0$ in 3-ZNRs and the difference between G_t^{ap} of even- and odd-width ZNRs enlarges as the width increases. In the insets of Fig. 2(a,b), we plot also the variation of G_t^{ap} versus M under U_0 of different strengths to show its dependence. At any finite M, G_t^{ap} increases (decreases) from zero ($2G_0$) and saturates to $2G_0$ (zero) for even (odd) n as U_0 increases (see also the insets of Fig. 1(f,g) and Figure S1).

The corresponding magnetoresistances R_M versus M are shown in Fig. 2(c,d) for even and odd n, respectively. Under $U_0 = t$, R_M is well below 10% for all even n and above 60% for all odd n in the range $M \in [0, 0.2]t$. When the energy of the bound state confined by U_0 in the p configuration is close to the Fermi energy, R_M can be negative for even n and shows an extra dip for odd n.

Using the density functional theory combined with the nonequilibrium Green's function implemented in the ATK package[39,40], we have simulated the transmission spectrum of hydrogen-passivated 4-ZGNRs and 5-ZGNRs substitutionally doped by a boron atom at edge site 0. The result agrees well with that from the tight-binding model of parameters $M = 0.07\,t$, $U_0 = 1.15\,t$ for 4-ZGNR and $M = 0.08\,t$, $U_0 = 1.20\,t$ for 5-ZGNR with $t = 2.7$ eV as shown in Figure S2. The magnetoresistance switch effect can be quite robust in real materials like ZGNRs. In the insets of Fig. 2(c,d), we plot R_M versus the temperature T for 4-ZNRs and 5-ZNRs with parameters close to those of the above boron doped ZGNRs, i.e. $U_0 = t$ and $M = 0.1\,t$. The behaviors of perfect/doped and even/odd ZNRs remains well distinguished from each other up to the room temperature $T = 0.01\,t/k_B$.

In the simplest case of 2-ZNR structure with $m = 0$, we have the analytical transmission expressions $\tau_\sigma^p(0) = [a_\sigma + U_0^2 \sin^2(\theta/2)]/(a_\sigma + U_0^2)$ and $\tau_\sigma^{ap}(0) = U_0^2 \sin^2(\theta/2)/[2Mt + U_0^2 \sin^2(\theta/2)]$ with $a_\sigma = 8Mt \sin^2\theta + 4\lambda_\sigma U_0\sqrt{2Mt}\sin\theta\sin(\theta/2)$ and $\cos\theta = M/4t$. They may be helpful for qualitative analysis in more general contexts. For $M = 0.1\,t$, the zero temperature magnetoresistance decreases from $R_M = 100\%$ at $U_i = 0$ to $R_M = -22.1\%$ at $U_0 = t$ similar to the result presented in Fig. 2(c) with $m = 5$ (see Figure S3 for the details).

If the potential shifts from site 0 to a site $i > 0$ where a downward residual magnetization M_i exists, the two-fold rotation symmetry of the system is broken and the transmission becomes spin dependent. The spin thermopower in the ap configuration can be greatly enhanced and shows strong even-odd effects on the nanoribbon width.

In even-width nanoribbons the spin-up (down) transmission peak shifts accordingly from $\varepsilon_\sigma^{\max} \approx 0$ to $\varepsilon_\uparrow^{\max} \approx M_i$ ($\varepsilon_\downarrow^{\max} \approx -M_i$) as shown in Fig. 3(a) for $U_2 = t$, $n = 4$, $i = 2$, and $M_2 = iM/(m+1) = 0.033\,t$ with

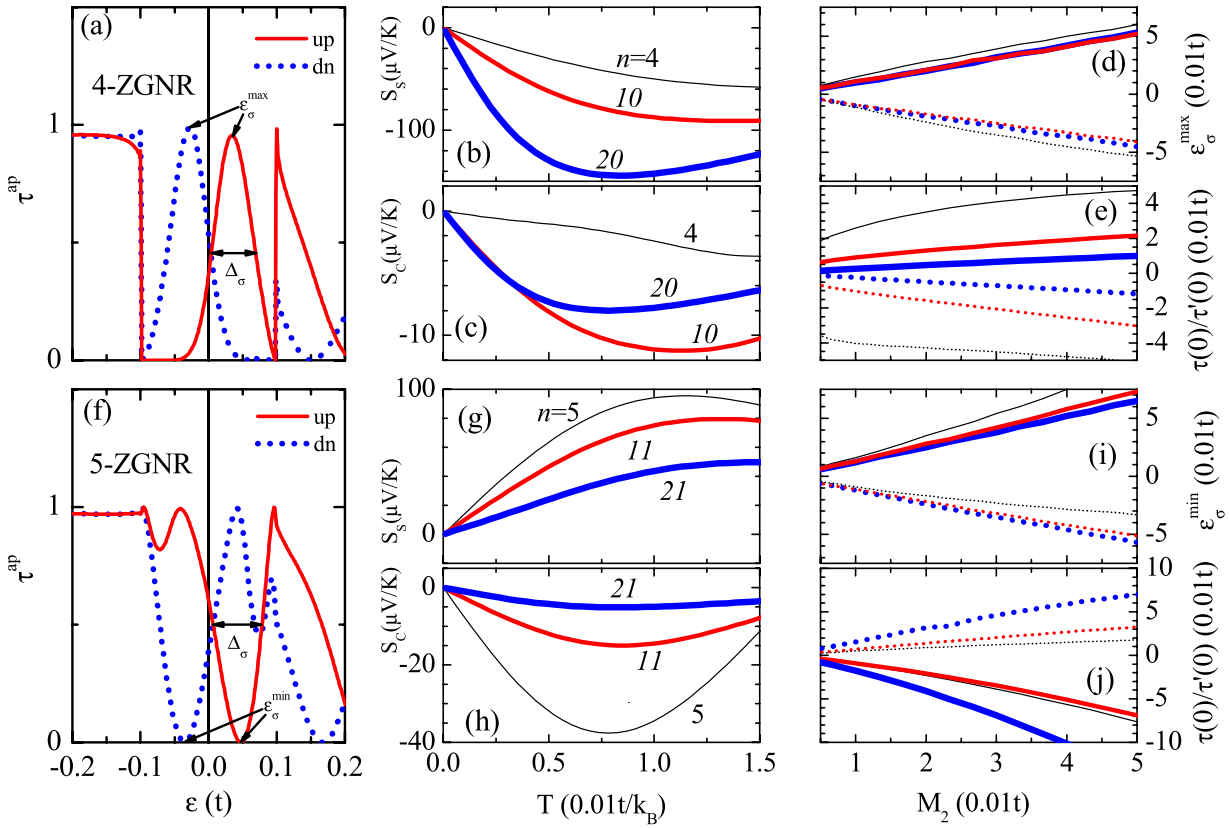

Figure 3. (**a**) $\tau_{\uparrow}^{ap}$ (solid) and $\tau_{\downarrow}^{ap}$ (dotted) of a 4-ZNR under a potential $U_2 = t$ at edge site 2. (**b**,**c**) S_S and S_C versus the temperature T, respectively, of n-ZNRs for even $n = 4$ (thin), 10 (medium), and 20 (thick) at $U_2 = t$ and $M = 0.1\,t$. (**d**) $\varepsilon_\sigma^{\max}$ and (e) $\tau_\sigma(0)/\tau'_\sigma(0)$ of up (solid) and down (dotted) spins are plotted versus the local edge magnetization M_2 for $n = 4$ (thin), 10 (medium), and 20 (thick) as M varies. (**f–j**) The same as in (**a–e**) for odd $n = 5$, 11, 21 with $\varepsilon_\sigma^{\max}$ replaced by $\varepsilon_\sigma^{\min}$.

$M = 0.1\,t$ and $m = 5$. The transmission spectrum then has a positive $\tau_\uparrow'(0)$ (negative $\tau_\downarrow'(0)$) which results in a negative $S_\uparrow$ (positive $S_\downarrow$) at low temperature according to the Mott formula. Interestingly, the spin Seebeck coefficient appears usually much greater than the charge one, i.e. $|S_S| \gg |S_C|$, because the transmission peaks of up and down spins are located almost symmetrically beside the Fermi energy, i.e. $\tau_\uparrow'(0) \approx -\tau_\downarrow'(0)$ and $\tau_\uparrow(0) \approx \tau_\downarrow(0)$. S_S can be further enhanced in wider nanoribbons where the transmission peaks become sharper with bigger $|\tau'(0)|$ and smaller $\tau(0)$.

The temperature dependent S_S and S_C plotted in Fig. 3(b,c), respectively, indicate that the Mott formula is valid below the critical temperature $T_c = \tau(1-\tau)/\tau' k_B|_{\varepsilon=0}$ which is determined by the width Δ_σ and the position $\varepsilon_\sigma^{\max}$ of the transmission peak. At high temperature the Seebeck coefficients decay gradually with the temperature due to the nonlinearity of the transmission spectrum.

The Seebeck coefficients can also be manipulated by the full magnetization M since both $|\varepsilon_\sigma^{\max}|$ and Δ_σ increase with M. As illustrated in Fig. 3(d,e) for $i = 2$, the variation of $\tau(0)$ is limited due to the opposite effects from increase of $|\varepsilon_\sigma^{\max}|$ and Δ_σ but $|\tau'(0)|$ decreases quickly and results in the decrease of S_σ. On the other hand, if the potential shifts from site 2 to site 3 while M remains fixed, $|\varepsilon_\sigma^{\max}|$ increases since $M_3 > M_2$, S_S then increases with the decrease of $\tau(0)$.

In odd-width nanoribbons, the spin-up (down) transmission dip shifts from $\varepsilon_\sigma^{\min} \approx 0$ to $\varepsilon_\uparrow^{\min} \approx M_i$ ($\varepsilon_\downarrow^{\min} \approx -M_i$) when the potential moves from site 0 to a site $i > 0$ as shown in Fig. 3(f) for $n = 5$. The dip width Δ_σ increases with $\frac{M}{m}$ but decreases with n. We have $\tau_\uparrow'(0) < 0 (\tau_\downarrow'(0) > 0)$ and then a positive S_S rather than the negative one in even-width nanoribbons. S_S decreases with i since the corresponding increase of $|\varepsilon_\sigma^{\min}|$ enhances $\tau(0)$. S_S decreases also with M because the increase of both Δ_σ and $|\varepsilon_\sigma^{\min}|$ reduces $\tau'(0)$ as shown in Fig. 3(j). If n increases, S_S becomes weaker further as illustrated in Fig. 3(g) when the decrease of Δ_σ leads to competing larger $\tau'(0)$ and larger $\tau(0)$. Different from the cases in even-width ZNRs, as shown in Fig. 3(i,j), $\varepsilon_\sigma^{\min}$ and $\tau_\sigma(0)/\tau'_\sigma(0)$ are more sensitive to n in odd-width ZNRs.

Summary

Zigzag nanoribbons of graphene-like materials are expected very useful for spintronics due to their edge spin polarization or magnetism. Giant magnetoresistance exists in pristine even-width ferromagnetic nanoribbons. With the help of an atomistic gate potential or edge disorder, the giant magnetoresistance can be switched off

(on) in even- (odd-) width nanoribbons. This originates from the jump of electronic transmission at the Fermi energy from zero to near 100% or verse vise in the antiparallel magnetic configuration if the potential is located at the transition interface of magnetization. If the potential shifts from the interface, the transmission peaks or dips of opposite spins split symmetrically beside the Fermi energy. The spin thermopower then becomes very large according to the Mott formula showing strong magneto-thermopower effect. This suggests that spin current can be produced from temperature gradient in the material.

References

1. Baibich, M. N., Broto, J. M., Fert, A., Nguyen Van Dau, F. & Petroff, F. Giant Magnetoresistance of (001)Fe/(001)Cr Magnetic Superlattices. *Phys. Rev. Lett.* **61,** 2472–2475 (1988).
2. Binasch, G., Grunberg, P., Saurenbach, F. & Zinn, W. Enhanced magnetoresistance in layered magnetic structures with antiferromagnetic interlayer exchange. *Phys. Rev. B* **39,** 4828–4830 (1989).
3. Prinz, G. A. Magnetoelectronics. *Science* **282,** 1660–1663 (1998).
4. Uchida, K. *et al.* Observation of the spin Seebeck effect. *Nature* **455,** 778–781 (2008).
5. Jaworski, C. M., Myers, R. C., Johnston-Halperin, E. & Heremans, J. P. Giant spin Seebeck effect in a non-magneticmaterial. *Nature* **487,** 210–213 (2012).
6. Walter, M. *et al.* Seebeck effect in magnetic tunnel junctions. *Nature Mater.* **10,** 742–746 (2011).
7. Bai, J. *et al.* Very large magnetoresistance in graphene nanoribbons. *Nature Nanotech.* **5,** 655–659 (2010).
8. Muñoz-Rojas, F., Fernández-Rossier, J. & Palacios, J. J. Giant Magnetoresistance in Ultrasmall Graphene Based Devices. *Phys. Rev. Lett.* **102,** 136810-1-4 (2009).
9. Zhang, Y. T., Jiang, H., Sun, Q. F. & Xie, X. C. Spin polarization and giant magnetoresistance effect induced by magnetization in zigzag graphene nanoribbons. *Phys. Rev. B* **81,** 165404-1-6 (2010).
10. Kim, W. Y. & Kim, K. S. Prediction of very large values of magnetoresistance in a graphene nanoribbon device. *Nature Nanotech.* **3,** 408–412 (2008).
11. Wang, Z. F. & Liu, F. Giant magnetoresistance in zigzag graphene nanoribbon. *Appl. Phys. Lett.* **99,** 042110-1-3 (2011).
12. Xu, C. *et al.* Giant magnetoresistance in silicene nanoribbons. *Nanoscale* **4,** 3111–3117 (2012).
13. Zhai, M. X. *et al.* Giant magnetoresistance and spin Seebeck coefficient in zigzag a-graphyne nanoribbons. *Nanoscale* **6,** 11121–11129 (2014).
14. Chen, A. B. *et al.* Spin-dependent ballistic transport properties and electronic structures of pristine and edge-doped zigzag silicene nanoribbons: large magnetoresistance. *Phys. Chem. Chem. Phys.* **16,** 5113–5118 (2014).
15. Zeng, M., Huang, W. & Liang, G. Spin-dependent thermoelectric effects in graphene based spin valves. *Nanoscale* **5,** 200–208 (2013).
16. Liu, Y. S., Wang, X. F. & Chi, F. Non-magnetic doping induced a high spin-filter efficiency and large spin Seebeck effect in zigzag graphene nanoribbons. *J. Mater. Chem. C* **1,** 8046–8051 (2013).
17. Novoselov, K. S. *et al.* Electric Field Effect in Atomically Thin Carbon Films. *Science* **306,** 666–669 (2004).
18. Tombros, N., Jozsa, C., Popinciuc, M., Jonkman, H. T. & van Wees, B. J. Electronic spin transport and spin precession in single graphene layers at room temperature. *Nature* **448,** 571–574 (2007).
19. Ruffieux, P. *et al.* On-surface synthesis of graphene nanoribbons with zigzag edge topology. *Nature* **531,** 489–492 (2016).
20. Magda, G. Z. *et al.* Room-temperature magnetic order on zigzag edgesof narrow graphene nanoribbons. *Nature* **514,** 608–611 (2014).
21. Fujita, M., Wakabayashi, K., Nakada, K. & Kusakabe, K. J. Peculiar localized state at zigzag graphite edge. *Phys. Soc. Jap.* **65,** 1920–1923 (1996).
22. Fernández-Rossier, J. Prediction of hidden multiferroic order in graphene zigzag ribbons. *Phys. Rev. B* **77,** 075430-1-5 (2008).
23. Son, Y. W., Cohen, M. L. & Louie, S. G. Energy Gaps in Graphene Nanoribbons. *Phys. Rev. Lett.* **97,** 216803-1-4 (2006).
24. Pisani, L., Chan, J. A., Montanari, B. & Harrison, N. M. Electronic structure and magnetic properties of graphitic ribbons. *Phys. Rev. B* **75,** 064418-1-9 (2007).
25. Georgakilas, V. *et al.* Functionalization of graphene: covalent and non-covalent approaches, derivatives and applications. *Chem. Rev.* **112,** 6156–6214 (2012).
26. Martins, T. B., Miwa, R. H., da Silva, A. J. R. & Fazzio, A. Electronic and transport properties of boron-doped graphene nanoribbons. *Phys. Rev. Lett.* **98,** 196803-1-4 (2007).
27. Wong, D. *et al.* Characterization and manipulation of individual defects in insulating hexagonal boron nitride using scanning tunneling microscopy. *Nature Nanotech.* **10,** 949–953 (2015).
28. Stroscio, J. A. & Eigler, D. M. Atomic and molecular manipulation with the scanning tunneling microscope. *Science* **254,** 1319–1326 (1991).
29. Díez-Pérez, I. *et al.* Rectification and stability of a single molecular diode with controlled orientation. *Nature Chem.* **1,** 635–641 (2009).
30. Cretu, O. *et al.* Electrical Transport Measured in Atomic Carbon Chains. *Nano Lett.* **13,** 3487–3493 (2013).
31. Rocha, A. R., Martins, T. B., Fazzio, A. & da Silva, A. J. R. Disorder-based graphene spintronics. *Nanotechnology* **21,** 345202-1-6 (2010).
32. Datta, S. *Quantum Transport: Atom to transistor.* (England: Cambridge University Press 2005).
33. Rejec, T., Ramšak, A. & Jefferson, J. Spin-dependent thermoelectric transport coefficients in near perfect quantum wires. *Phys. Rev. B* **65,** 235301-1-5 (2002).
34. Heiliger, C., Zahn, P. & Mertig, I. Microscopic origin of magnetoresistance. *Mat. Today* **9,** 46–54 (2006).
35. Cutler, M. & Mott, N. F. Observation of Anderson Localization in an Electron Gas. *Phys. Rev.* **181,** 1336–1340 (1969).
36. Mott, N. F. & Davis, E. A. *Electronic Processes in Non-Crystalline Materials.* (New York: Oxford University Press 2012).
37. Sivan, U. & Imry, Y. Multichannel Landauer formula for thermoelectric transport with application to thermopower near the mobility edge. *Phys. Rev. B* **33,** 551–558 (1986).
38. Paulsson, M. & Datta, S. Thermoelectric effect in molecular electronics. *Phys. Rev. B* **67,** 241403-1-4 (2003).
39. Taylor, J., Guo, H. & Wang, J. Ab initio modeling of open systems: Charge transfer, electron conduction, and molecular switching of a C60 device. *Phys. Rev. B* **63,** 121104-1-4 (2001).
40. Brandbyge, M., Mozos, J. L., Ordejón, P., Taylor, J. & Stokbro, K. Density-functional method for nonequilibrium electron transport. *Phys. Rev. B* **65,** 165401-1-17 (2002).
41. Li, T. C. & Lu, S. P. Quantum conductance of graphene nanoribbons with edge defects. *Phys. Rev. B* **77,** 085408-1-8 (2008).

Acknowledgements

We appreciate Hong Guo and Yu-Shen Liu for helpful discussion. This work was supported by National Natural Science Foundation of China (Grant Nos 61674110 and 91121021).

Author Contributions

M.-X.Z. and X.-F.W. designed research, performed research, analyzed data, and wrote the paper.

Additional Information

Supplementary information accompanies this paper at http://www.nature.com/srep

Competing financial interests: The authors declare no competing financial interests.

How to cite this article: Zhai, M.-X. and Wang, X.-F. Atomistic switch of giant magnetoresistance and spin thermopower in graphene-like nanoribbons. *Sci. Rep.* **6**, 36762; doi: 10.1038/srep36762 (2016).

Publisher's note: Springer Nature remains neutral with regard to jurisdictional claims in published maps and institutional affiliations.